*Journal of Earth Sciences and Geotechnical Engineering, Vol. 15, No. 1, 2025, 39-69*
*ISSN: 1792-9040 (print version), 1792-9660 (online)*
*https://doi.org/10.47260/jesge/1512*
*Scientific Press International Limited*

# Numerical Analysis of the Large-scale Dynamic Test of Rock Support at Kiirunavaara mine – Improved Design

**Shirzadegan Shahin[1], Warema Senzia[2], Nordlund Erling[2], Zhang Ping[2] and Yi Changping[2]**

## Abstract

The numerical analysis results from an improved design of large-scale dynamic test of rock support (Test 6) is presented in this paper. The improved field test was designed based on the results obtained from field tests and the numerical analysis of the earlier tests (Tests 1 – 5) conducted at LKAB Kiirunavaara mine. The performed numerical analysis investigates how the improvements including minimizing the expansion of blasting gases into the burden, avoiding the complete damage of the burden, and creating sub-planar waves were achieved under the improved design of the test. Furthermore, the response of supported and unsupported excavations as well as the complex interaction of stress waves and rock support was numerically studied. The numerical analysis comprised of two stages (i) the explosion stage modelled with the finite element code LS-DYNA and (ii) the wave propagation stage which was modelled using UDEC with the results from LS-DYNA as input. The accuracy of the developed models was investigated by comparison of the UDEC models results to the data obtained from the field test. The numerical analysis results confirmed that the improved designed burden has assisted in reducing the areas of tensile yielding in the burden and as a result, the gas expansion and complete damage of the burden was avoided. The simulation results showed that the used support system (Swellex Mn 24 and reinforced shotcrete) has effectively limited the displacement of the test wall and prevented ejection during the dynamic loading. The combined numerical technique has shown its advantage when simulating blasting as well as interaction between waves and opening and it can thus be used as a tool for evaluating rock support performance.

**Keywords:** Numerical analysis, Large-scale test, Dynamic rock support, UDEC, LS-DYNA.

[1] Ramboll Sweden AB, Rock Engineering Division.
[2] Luleå University of Technology.

Article Info: Received: September 25, 2024. Revised: November 1, 2024.
Published online: January 9, 2025.

# 1. Introduction

Large-scale test of rock support have been carried out in different mines worldwide aiming to improve the understanding and quantify the performance of support systems (Ortlepp, 1969; Ortlepp, 1992; Tannant et al,. 1994; Tannant et al., 1995; Ansell, 1999; Hagan et al., 2001; Espley et al., 2002; Archibald et al,. 2003; Ansell, 2004; Andrieux et al., 2005; Heal et al., 2005; Heal and Potvin, 2007; Heal, 2010; Shirzadegan et al., 2016a; Shirzadegan et al., 2016b). In this testing method, the support system is dynamically loaded by means of a nearby blast.

Despite the cost and practical complications, a well-designed large-scale test of rock support, can facilitate in-situ dynamic testing of support systems (Hadjigeorgiou and Potvin, 2007; Potvin et al., 2010; Stacey, 2011; Stacey ,2012). Different test designs used by different researchers have led to various levels of success in evaluating the performance of the installed rock support. Hadjigeorgiou and Potvin (2007) suggested that standardizing the procedure of the large-scale tests, and increasing the database of the results, will be a step forward to better understand the capability of dynamic resistant support systems.

Within this context, the numerical analysis of a large-scale test of rock support, Test 6 (Shirzadegan et al., 2016b) conducted at LKAB Kiirunavaara mine, is carried out and presented in this paper to contribute in developing a field and numerical method for the design of in-situ dynamic testing of rock support. The design of field Test 6 was based on the findings in field Tests 1 – 5 (Shirzadegan et al., 2016a), and the preliminary numerical analysis of Tests 2 and 5 conducted by Zhang et al. (2013). Results from Tests 1 – 5 showed that in Tests 1 and 2, despite high values of PPV calculated through accelerometers recording, the induced damage to the rock support and test wall was minimal, while in Tests 4 and 5, the complete burden was damaged, despite the burden was designed in a range similar to that in Tests 1 and 2 (Shirzadegan et al., 2016a). The results from field Tests 1 – 5, and the preliminary numerical analysis of Tests 2 and 5, conducted by Zhang et al. (2013), led to the conclusion that the response of the wall is sensitive to the choice of burden. Based on these suggestions, the design of the burden in Test 6 was revised.

The results in field Test 6, seemed to show that the new burden design was successful to mimic a semi-planar wave front, similar to that from a real seismic event (Shirzadegan et al., 2016b). A summary of field Test 6 is presented in section 2. In this paper, in order to increase the understanding of the improved design of the large-scale Test 6, numerical analyses of this test were carried out. The aim was to study in more detail (i) the behaviour of rock mass in the burden and at the test wall, and (ii) the performance of the rock support for the improved design in Test 6.

The numerical analysis technique which was used to the develop the models of Test 6, was a combination of the finite element code LS-DYNA and the distinct element code, UDEC. A literature review of similar modelling technique used by other researchers, and a description of this technique are presented in section 3. The numerical analyses of Test 6 considered a number of factors including the effect of geological structures, rock support, and blasthole and charge geometry. Four

different models were developed, based on the geological report of the site where Test 6 was carried out. The numerical analyses results of the models were compared to the data obtained from field Test 6 in terms of velocity – time, maximum displacement, and the ejection thickness from the wall to evaluate the numerical models. The model that calculated results closer to the field monitoring data was chosen to study the behaviour of the rock mass and the rock support in field Test 6. At the end, the advantageous and disadvantageous of the of large-scale tests of rock support are discussed based on the experiences and findings gained during field tests conducted at LKAB Kiirunavaara mine and their associated numerical analysis.

### 1.1 Kiirunavaara Mine Description

Kirunavaara Mine where the field tests were carried out is large scale underground iron ore mine located in the north part of Sweden, presented in Figure 1. Its orebody is inclined and dips 60 degree to the east. The orebody is estimated to be 4km deep with average width of 80m. The mining method deployed is sub-level caving and production activities in the mine are at levels deeper than 1km.


**Figure 1: Location of the Mine Site.**

## 2. Design in field Test 6

In order to design a burden that assist in minimizing the blasting gas effect, and avoiding too much geometrical damping of the induced wave, two blastholes were suggested to be drilled in the middle of the 16 m wide pillar between two cross-cuts (100 and 103). The burden (the distance of the blasthole to the side wall in each cross-cut) varied along the tested sidewalls due to the deviation of the blastholes combined with the irregular surface of the tested walls. 0 illustrates the plan view of the test site.

During Test 6, one of the blastholes did not detonate, therefore only the detonated blasthole is illustrated in 02. The position of this hole above the floor of the footwall drift was 3.3 m. The burdens at sections A, B, C, D and E, where the monitoring instruments were installed, is presented in 02. The spacing between the sections is 2 m. The length of the drilled blasthole was 20 m, and the diameter was 152 mm. The hole was charged with NSP711 with a length of 10 m and a diameter of 120 mm. No stemming material was used to vent and reduce the effect of detonation gases.

In cross-cut 100, the test wall was supported by a dynamic rock support system comprising 100 mm fibre reinforced shotcrete (40 kg /$m^3$ steel fibre), 75 mm × 75 mm weld mesh with 5.5 mm diameter and Swellex Mn 24 rockbolts in a 1 m × 1 m pattern. The length of the supported wall was 20 m. The test wall in cross-cut 103, was only supported by the plain shotcrete. The plain shotcrete in cross-cut 103 was sprayed during the development many years ago. Therefore, the test wall in cross-cut 103 was assumed to be unsupported considering the deterioration of the shotcrete. Having one cross-cut supported, the other unsupported, and the blasthole drilled almost in the middle of the pillar, provided the opportunity to evaluate the performance of the installed support system, by comparing the damage intensity between the two cross-cuts. The results from field Test 6 were described in detail by Shirzadegan et al. (2016b).

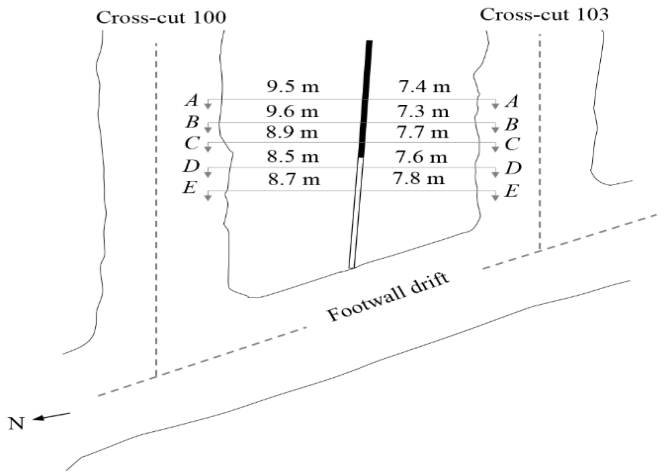


**Figure 2: Plan view of the Test 6. The burden from the blasthole to each cross-cut is specified for different sections.**

## 2.1 Geological information and joints properties

Geological investigations of the test site were conducted by Andersson (2010). The area was characterized by an intense network of geological structures in many directions. The joint spacing was generally in the range of 1 m - 3 m. Three major joint sets 1, 2a, and 3a (see 0) were identified in the test area (Andersson 2011). Since set 2a has an strike perpendicular to the tunnel direction, only sets 1 and 3a were considered for the two dimensional numerical analysis.

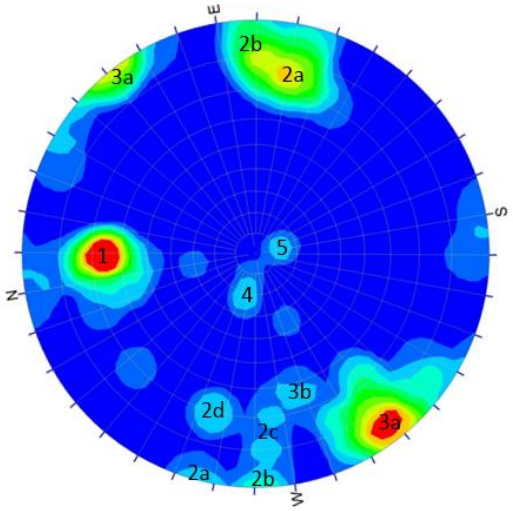


**Figure 3: Pole density plot for the joint sets in the pillar between cross-cuts 100 and 103 (Andersson 2011).**

As the analysis was conducted with a two-dimensional numerical code, UDEC, it was necessary to calculate the apparent dip of the identified major joint sets. The apparent dip in terms of the true dip is expressed as:

$$\alpha = \arctan(\tan\delta \times \sin\beta) \tag{1}$$

where, $\delta$ is the true dip and $\beta$ is the angle between the strike of the structure and the plane of the cross section of interest. The orientation of the major joint sets and their associated apparent dip are presented in 0.

**Table 1: Major joint sets modelled in the UDEC model.**

| Set | Range of dip angle [°] | $\delta$ [°] | $\beta$ [°] | $\alpha$ [°] | Spacing [m] |
|---|---|---|---|---|---|
| 1: W-NW | 50-80 | 65 | 88 | 65* | 1-3 |
| 3a: N-NW | 60-90 | 75 | 39 | 66 | 1-3 |

* The input angle in UDEC for set 1 is set to 115 degrees due to its dip direction with respect to the cross-cuts direction.

The mechanical properties of the joints required for numerical analysis are the tensile strength, $\sigma_t$ , cohesion, $c$, the friction angle, $\phi$ and the shear and the normal stiffness, $k_s$ and $k_n$, respectively. The parameter values are from Malmgren and Nordlund (2006) and summarized in 0.

**Table 2: Mechanical properties of the joints (Malmgren and Nordlund, 2006).**

| $\phi$ [°] | $c$ [MPa] | $\sigma_t$ [MPa] | $k_n$ [GPa/m] | $k_s$ [GPa/m] |
|---|---|---|---|---|
| 35 | 0.5 | 0.5 | 9 | 9 |

### 2.2 Rock material properties

The values of density, $\rho$, Young's modulus, $E$, and Poisson's ratio, $v$ of the rock, used in the numerical analysis are from the earlier studies by Malmgren and Nordlund (2008) and are summarized in 0. Since the joint sets were considered in the models, intact rock properties were assumed for the blocks. Furthermore, the uniaxial compressive strength (UCS) of the intact rock was taken from Malmgren (2008) for the footwall rock type SP3 (LKAB´s internal designation). The tensile strength $\sigma_t$ , cohesion $c$, and friction angle, $\phi$, in 0 were obtained from Brandshaug (2009) using SP3 and Hoek-Brown parameters of intact rock given by Malmgren (2008) .i.e., GSI= 100, m = 31.4, and s = 1.

**Table 3: Intact rock properties used in the numerical analysis (Malmgren and Nordlund, 2008; Malmgren, 2008; Brandshaug, 2009).**

| Density $\rho$ [kg/m$^3$] | Young's modulus $E$ [GPa] | Cohesion $c$ [MPa] | Friction angle $\phi$ [°] | Tensile strength $\sigma_t$ [MPa] | Poisson's ratio $v$ | UCS [MPa] |
|---|---|---|---|---|---|---|
| 2800 | 70 | 31 | 61 | 16.5 | 0.27 | 267 |

## 3. Numerical modelling techniques

As it is not possible to model the blasting in UDEC, in this study LS-DYNA is used (i) to model the blast, (ii) to obtain the blasting load in form of velocity time from the crushed zone boundary (CZB) created around the blasthole, and (iii) to specify the diameter of the crushed zone. The velocity – time curve obtained from LS-DYNA is then applied in UDEC as an internal boundary load around the crushed zone.

In the following sections, first the modelling technique used by the other authors is briefly reviewed, and next the modelling process in LS-DYNA and UDEC in this study is described.

### 3.1 Review of the numerical modelling technique

In some of the earlier UDEC studies of blasting, the input including peak value, rise time and duration was estimated based on experiments. Examples are the works conducted by Rosengren (1993) and Senseny and Simons (1994).

Chen and Zhao (1998) used a coupled numerical model to study the blast wave propagation in jointed rock. In their study, the potential of using UDEC to model

blast wave propagation in a jointed rock mass using velocity input data from a finite difference program AUTODYN-2D was investigated. The conclusion was that the coupled model is capable of modelling the blast process and the response of a jointed rock mass. The approach was later used by Chen et al. (2000), Wang et al. (2009), Zhang et al. (2013), and Deng et al. (2015) to study the rock mass response to blasting loading.

Chen et al. (2000) used UDEC and AUTODYN numerical modelling to investigate the blast load characteristics and stress wave propagation in a jointed rock mass. In their study, the PPV was used as a measure of the damage. Therefore, the PPVs obtained from the UDEC and AUTODYN were compared to those measured in the field and those obtained from empirical equations proposed by Wu (1971). The results showed that the PPVs calculated using UDEC gave a better agreement with the field test PPVs than those obtained from the empirical equations. Chen et al. (2000) concluded that the analysis of the field test agreed well with the field test results and that the dynamic parameters play a significant role in modelling especially when the model is used to produce prediction results.

Wang et al. (2009) simulated an underground blast in a faulted rock mass. The combination of UDEC and LS-DYNA was used for the simulation. The principal aims of the study were to numerically study (i) the capability of UDEC and LS-DYNA in modelling the blast wave propagation in a faulted rock mass, (ii) the blast induced crack evolution and failure zone distribution around the blasthole, and (iii) the relationship between rock failure and the fault parameters such as orientation, stiffness and friction. Wang et al. (2009) concluded that, the coupled method was appropriate to study the effect of blasting in a discontinuous rock mass. It was shown that during the process of stress wave propagation, tensile stresses or compressive stresses caused rock material to fail in tension or in compression resulting in a crushed region close to the borehole. This was followed by a fractured zone, in which the rock was severely cracked.

Zhang et al. (2013) used a combination of LS-DYNA and UDEC to investigate the failure mechanisms in the large-scale simulated rockburst tests carried out at the Kiirunavaara mine (Shirzadegan et al., 2016a; Shirzadegan et al., 2016b) and improve the blast design. The finite element code, LS-DYNA, was used to calculate the location of the crushed zone boundary (CZB) created around the blasthole and the particle velocity time history at that boundary. The reason for defining the CZB is that the crushed zone absorbs a large amount of blasting energy, and cannot be modelled in UDEC correctly (Zhang et al., 2013). The wave propagation and the response of the rock mass outside the CZB, was modelled using UDEC. The particle velocity history at the CZB obtained from the LS-DYNA analysis was applied as an internal boundary condition in UDEC. They concluded that the blast induces (i) tangential tensile stresses at the front of the incident compressive wave. The tangential tensile stress can create radial fractures that propagates from the blasthole all the way to the surface of the test wall and (ii) radial tensile stresses, as a result of the reflection of the blast-induced wave at the test wall surface, that create fractures parallel or sub-parallel to the surface of the tested wall. The results assisted

to improve the design of future tests at LKAB Kiirunavaara mine.
In the analysis conducted by Deng et al. (2015) a large-scale decoupled underground explosion test in Älvdalen, Sweden was numerically analysed by combining AUTODYN and UDEC. The objective of the field test was to evaluate the underground facility design and to determine the hazard of underground ammunition storages (Chong et al., 2002). During the field test, the ground vibration on the side walls, roof, and inside the rock mass along the horizontal and vertical directions were measured. Deng et al. (2015) compared the peak particle velocity obtained from empirical estimations, AUTODYN modelling, and AUTODYN-UDEC modelling. The authors concluded that the empirical equations underestimate, and the AUTODYN analysis overestimates the particle velocity and that the AUTODYN-UDEC numerical analysis results agree well with the test data.

### 3.2 LS-DYNA model

LS-DYNA is a commercially available multi-purpose explicit and implicit finite-element code, which can be used to analyse the nonlinear response of structures to dynamic loading (Hallquist, 2006). In this study, the LS-DYNA-model featured a 10 m explosive column with the diameter 120 mm in a 20 m long blasthole. The diameter of the blasthole was 152 mm. The detonation process was simulated by a three-dimensional cylinder model with the length of 25 m and diameter of 20 m. Non-reflecting (i.e. viscous) boundaries were introduced around the outer perimeter of the domain to eliminate wave reflections. LS-DYNA uses an explosive material model combined with the Jones-Wilkins-Lee (JWL) equation of state to describe the detonation of explosive which is defined as (Hallquist, 2006):

$$P = X\left(1-\frac{w}{R_1 V}\right)e^{-R_1 V}+Y\left(1-\frac{w}{R_2 V}\right)e^{-R_2 V}+\frac{we}{V} \qquad (2)$$

where $P$ is the pressure (Pa) induced by detonation; $X$, $Y$, $R_1$, $R_2$ and $w$ are the user defined input parameters related to the used explosives; $V$ is the relative volume; and $e$ is the energy per unit volume of the explosive. The NSP 711 explosive used in the field test was simulated in the LS-DYNA analyses. The used values for the constants and parameters in Equation (2) are based on calibration analyses conducted on this type of explosive by Helte et al. (2006). The calibrated data are presented in 0. The detonation velocity of NSP711 is 7680 m/s (Helte et al., 2006) and the value of Chapman-Jouguet (C–J) pressure is equal to 21.15 (GPa).

**Table 4: Parameters of NSP 711 explosive (Helte et al., 2006).**

| $\rho_e$ [kg/m$^3$] | $X$ [GPa] | $Y$ [GPa] | $R_1$ | $R_2$ | $w$ | $e$ [GPa] |
|---|---|---|---|---|---|---|
| 1500 | 759.9 | 12.56 | 5.1 | 1.5 | 0.29 | 7.05 |

The charge in the blasthole was decoupled, and the gap between the explosive and the wall of the blasthole was filled with air. The air was considered as an ideal gas following the pressure–energy law:

$$P=(\gamma-1)\frac{\rho_e}{\rho_{e0}}e_0 \tag{3}$$

where $P$ is the gas pressure; $\gamma = 1.4$ is a constant (the ratio of specific heats); $\rho_e$ is the current air density; $\rho_{e0} = 1.29$ kg/m$^3$ is the initial gas density; and $e_0$ is the specific internal energy and assumed to be 0.25 MPa. The ideal gas values are determined according to Olovsson et al. (2003).

The rock mass is modelled with the RHT material model which is an advanced plasticity model for brittle materials such as concrete and rock (Riedel et al., 1999), implemented in LS-DYNA (Borrvall and Riedel 2011). In the RHT model, the description of the stress state is based on the three invariants of the stress tensor for the definition of the elastic limit surface, failure surface and residual strength surface for the crushed material. These three surfaces are all pressure dependent. The values of some parameters required for modelling of the rock in LS-DYNA are presented in 0. The RHT model includes a damage model based on continuum damage theory (Hallquist, 2006). In LS-DYNA, the crushed zone can be identified by the damage level as the embedded RHT model can simulate both tensile and compressive failure with a damage model. The damage is defined using:

$$D=\sum\frac{\Delta\varepsilon^p}{\varepsilon^f} \tag{4}$$

where $\Delta\varepsilon^p$ is the accumulated plastic strain and $\varepsilon^f$ is the failure strain.

0 shows the calculated damage level around the blasthole in LS-DYNA. The crushed zone around the blasthole is shown in 0 and it is represented by the red colour. The calculated diameter of the crushed zone was 1.1 m. The recorded wave monitored at the CZB is represented by the velocity-time curve presented in 0. The area near the crushed zone marked in green colour in 0 was interpreted as the fractured zone.

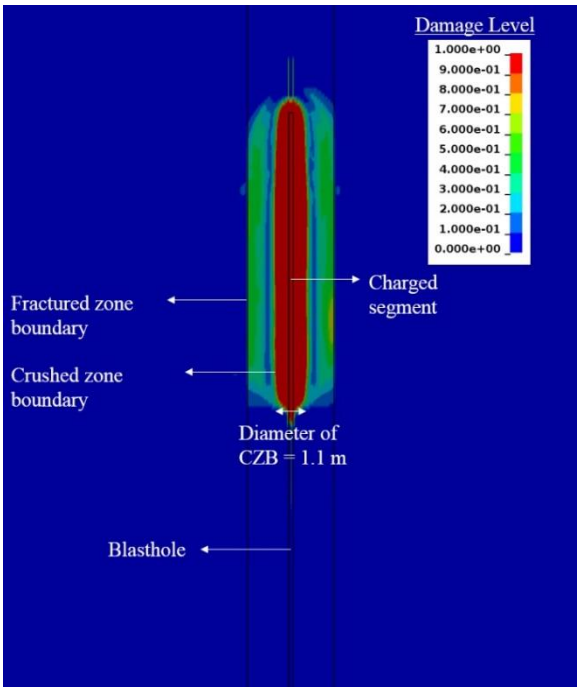


**Figure 4: Identification of crushed zone boundary in LS-DYNA.**

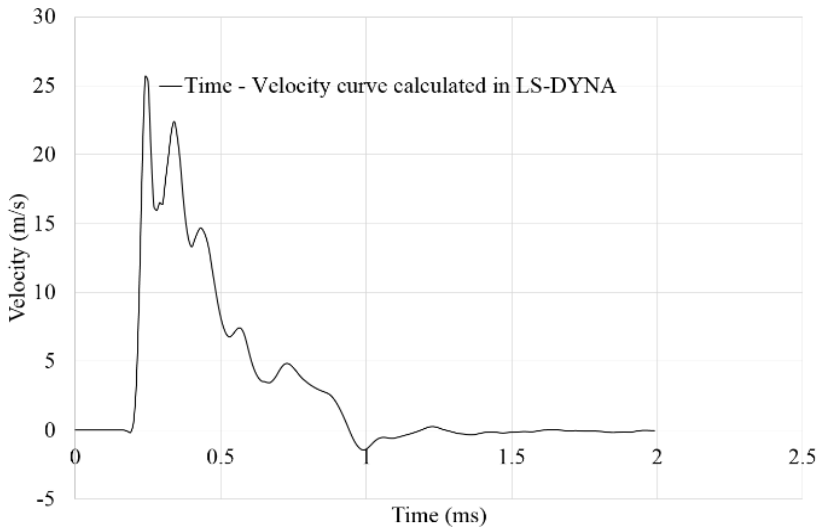


**Figure 5: Velocity – time calculated in LS-DYNA at the boundary of the identified crushed zone.**

## 3.3 UDEC model

### 3.3.1 Model description

The distinct element code UDEC is designed to solve discontinuous problems (Itasca Consulting Group 2015). The code is widely used to study the wave propagation through a jointed rock mass (Lemos, 1997; Zhao et al., 2008; Barla et al., 2010).

The model constructed in UDEC was 80 m × 80 m and included cross-cuts 100 and 103 and the crushed zone boundary (CZB) with a diameter of 1.1 m. The width and height of cross-cuts 100 and 103, were 7 m and 5.2 m, respectively. 0 shows the general configuration of the UDEC model. The burdens (distance from the centre of the CZB to the walls of cross-cuts 100 and 103) were defined according to section C-C presented in 0. In this section all accelerometers in both cross-cuts had satisfactory recordings. The orientation of the two major joint sets defined in the model were according to the data listed in 0, and the joints and the rock material properties were according to the data presented in 0 and 0.

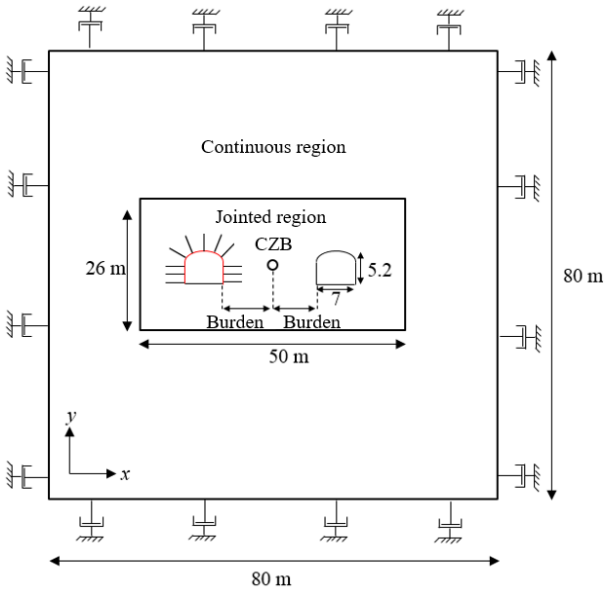


**Figure 6: The geometry of the UDEC model.**

Considering the P-wave velocity of the rock material 5589 m/s and the dominant frequency of 195 Hz, the wave length will be approximately 29 m. According to Kuhlemeyer and Lysmer (1973), the mesh ratio (a ratio of the maximum element length to the wave length) should be smaller than 1/8-1/12 to ensure numerical accuracy of wave propagation problems. According to Deng et al. (2015), at least three layers of zones should lie between the adjacent joints to balance between computational accuracy and efficiency. For this purpose, the zone edge length is set to 0.2 m to have at least five layers of zones between adjacent joints.

The model was solved in two steps; i.e. static and dynamic. In the static part, zero displacement boundary condition was defined for the external boundaries. The assigned in situ stresses were according to a previous mine-scale numerical analysis of the Kiirunavaara mine by Malmgren and Sjöberg (2006). Based on this analysis, the stress determined at the mining level 741 m were 16.5 MPa and 11.3 MPa along the *x* and *y* directions, respectively. In the static part, the model was run with elastic material properties until equilibrium before and after the excavation. Then the plastic material properties were assigned and the models are solved. Next in the dynamic part of the model, non-reflecting (i.e. viscous) boundaries were introduced around the outer perimeter of the domain to eliminate wave reflections. At this stage The calculated velocity wave form in LS-DYNA was applied to the CZB (radius of 0.55 m) as an internal boundary condition.

### 3.3.2 Rock support

The installed rock support in Test 6 was modelled numerically. The aim was to simulate conditions which are as close as possible to the conditions in the field. In the field Test 6, 100 mm thick reinforced shotcrete (40 kg/m$^3$ steel fibre) was sprayed on the surface of the test wall in cross-cut 100. In the field test, weld mesh was also installed over the surface of shotcrete, but its effect is not considered in UDEC analysis.

UDEC has the capability to simulate surface support using two types of structural elements including structural beam elements and support members (Itasca Consulting Group 2015). In this study, the structural (beam) element method was used to model the fibre reinforced shotcrete. This material model can simulate inelastic behaviour that is representative of common surface lining materials, e.g. non-reinforced and reinforced cemented materials (Itasca Consulting Group 2015). The mechanical properties of the fibre reinforced shotcrete used in the models are summarized in 0. The properties were determined based on a series of laboratory studies conducted by Malmgren (2007). Malmgren (2007) provided a value range for the determined mechanical properties summarized in 0. However, in this study, the average values from these tests were used for the modelling.

**Table 5: Mechanical properties of reinforced shotcrete (Malmgren, 2007).**

| Density [kg/m$^3$] | Poisson's ratio | Uniaxial compressive strength [MPa] | Tensile strength [MPa] | Residual tensile yield strength [MPa] | Young's modulus [GPa] |
|---|---|---|---|---|---|
| 2300 | 0.15 | 35 | 3.8 | 3.1 | 19 |

The second set of parameters that need to be specified to model the structural elements are the interface material properties. Direct shear tests, and complementary tension and compression tests were conducted by Saiang et al. (2005) on rock-shotcrete interfaces to assess the strength and stiffness of interface. The interface properties based on the study by Saiang et al. (2005) are summarized in 0.

**Table 6: Mechanical properties of shotcrete and rock interface (Saiang et al., 2005).**

| Normal stiffness [GPa/m] | Shear stiffness [GPa/m] | Cohesion [MPa] | Tensile strength [MPa] | Friction angle [degree] |
|---|---|---|---|---|
| 250 | 1 | 0.6 | 0.6 | 35 |

In this study, the Rockbolt element capable of providing bending resistance behaviour was used to model the rockbolts. The simulated elements can yield under axial loads, and can resemble rockbolt failure based on the tensile failure strain limit defined by the user (Itasca Consulting Group 2015).
The geometrical specifications, mechanical properties, and the interface material properties of the Swellex rockbolt are summarized in 0, 0, and 0. The Swellex Mn 24 data are used from Epiroc product data, discussions with Epiroc representatives and a series of numerical pull-out test conducted by Shirzadegan (2020).

**Table 7: Geometrical specifications of Swellex Mn 24 (Shirzadegan, 2020).**

| Area [$m^2$] | Second moment of inertia [$m^4$] | Perimeter [m] |
|---|---|---|
| $3.27\times10^{-4}$ | $11.06\times10^{-8}$ | 0.151 |

**Table 8: Mechanical properties of Swellex Mn 24 (Shirzadegan, 2020).**

| Density [$kg/m^3$] | Young's modulus [GPa] | Tensile yield load [kN] | Tensile failure strain limit | Compressive yield load [kN] |
|---|---|---|---|---|
| 7800 | 200 | 240 | 0.35 | $2\times10^6$ |

**Table 9: Mechanical properties of rockbolt and rock interface (Shirzadegan, 2020).**

| Normal cohesive strength [N/m] | Normal stiffness [N/m/m] | Shear cohesive strength [N/m] | Shear stiffness [N/m/m] |
|---|---|---|---|
| $2\times10^9$ | $1\times10^9$ | $2\times10^5$ | $120\times10^6$ |

# 4. Numerical Model Calibration

In the simulation of Test 6, the two major joint sets presented in 0 were considered. Field geological investigations revealed that the joint spacing mapped around cross-cuts 100 and 103 were generally in the range of 1 – 3 m. As the exact spacing between each set was not reported, models with different joint spacing scenarios, S1 to S4 summarized in 0, were used in the simulations. The objective was to identify the joint spacing that provides velocities which are as close to those obtained in field Test 6 as possible. Furthermore, two models S5 and S6 were developed to study the increasing number of blastholes effect, and rock support performance.

In models S1, S2 and S3, the same joint spacing was used for the two joint sets (0). The spacing in model S4 was based on the suggestions during the geological investigations where the spacing for Set 1 was generally smaller than that of the other joint sets.

**Table 10: Joint spacing scenarios used in the numerical models of the Test 6.**

| Model | Spacing in Set 1 [m] | Spacing in Set 3 [m] |
|---|---|---|
| S1 | 1 | 1 |
| S2 | 2 | 2 |
| S3 | 3 | 3 |
| S4 | 1 | 2 |
| S5 | 1 | 1 |
| S6 | 1 | 1 |

In the models analysed in this paper the history points of the velocity and displacement in the test walls (three points in cross-cut 100 and one point in cross-cut 103) were monitored. The location of the history points in each section was identical to that of the installed accelerometers in Test 6. 0 shows the position of the history points in cross-cuts 100 and 103 in the UDEC model. It should be noted that the accelerometers in Test 6 were installed at a depth of 0.2 m from the surface of the shotcrete. Therefore, the histories in UDEC are also located at a depth of 0.2 m from the surface of the opening to coincide with the field measurements.

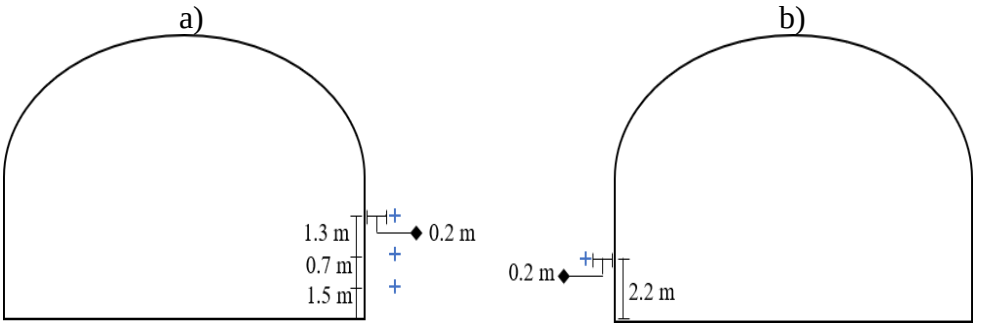


**Figute 7: Location of the history points in the UDEC model.**

The distribution of the accelerometers on the test walls in Test 6, cross-cuts 100 and 103, and their vertical distance from the floor are shown in 0a and b. The accelerometers were distributed along three rows, namely top, middle and bottom, in cross-cut 100, and along one row, middle, in cross-cut 103.
Sections A to F in cross-cuts 100 and 103 in 0a and b are identical to the sections presented in 0. In 0, the accelerometers represented by filled black circles are the ones that provided data, and those with un-filled black circles did not provide data. At the points where the installed accelerometers did not coincide with the defined sections, or did not provide data, the PPV was read from the PPV contour plot calculated by Shirzadegan et al. (2016b).

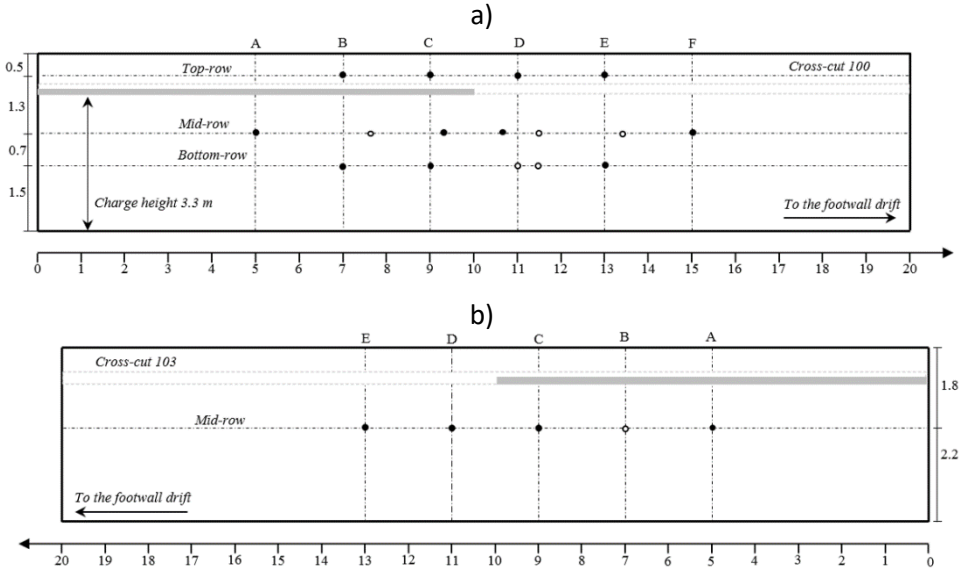


**Figure 8: Distribution of accelerometers over the tested walls by distance in [m] at a) cross-cuts 100, and b) cross-cut 103.**

## 4.1 PPV comparison between field and UDEC models

The computed PPVs and those measured in the field were compared for each row of the tested walls. The field measured PPVs at different sections along each row (top, middle, and bottom), together with the calculated PPVs by UDEC in section *C* are shown in 0a – d. The *x*-axis in each plot in 0 represents the distance from the end of the blasthole (corresponding to 0 on the *x*-axis in 0). The models which have calculated PPVs close to the field measurements along each row are summarized in 0.

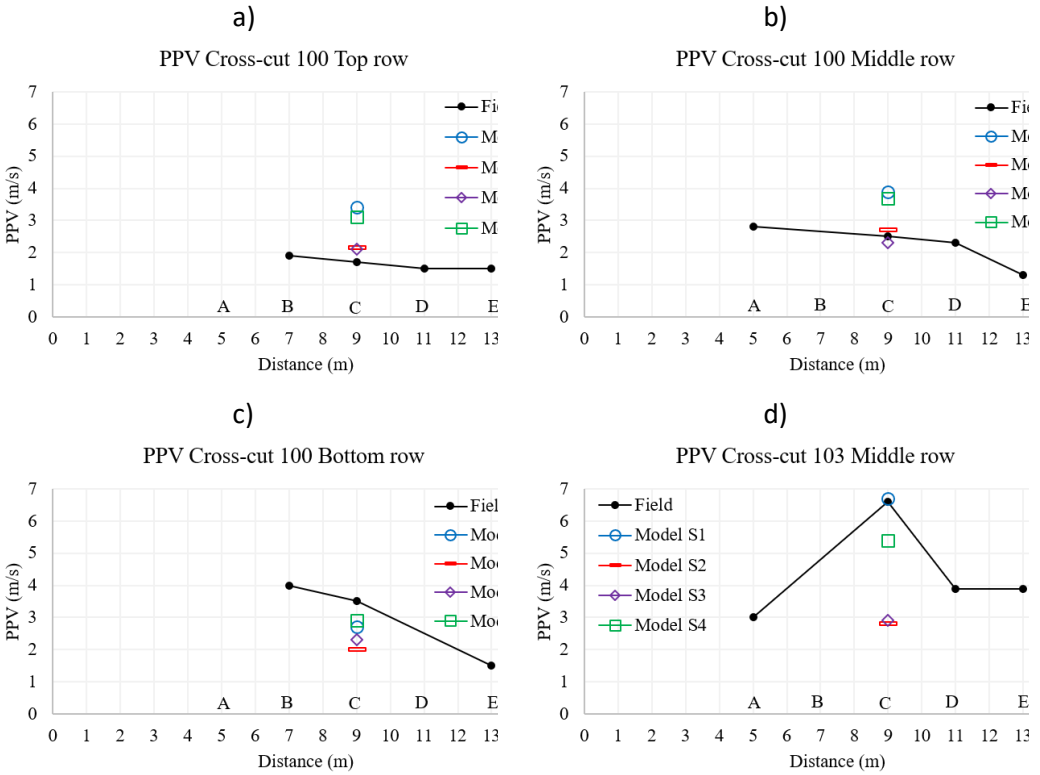


**Figure 9: Comparison of PPVs from the field test and the models with different joint spacings, a) cross-cut 100, top row, b) cross-cut 100, middle row, c) cross-cut 100, bottom row, d) cross-cut 103, middle row.**

**Table 11: Models with PPV close to field measurements along each row,**

| Cross-cut | Row | Models with PPV close to field measurements |
|---|---|---|
| 100 | Top | S2 and S3 |
| 100 | Middle | S2 and S3 |
| 100 | Bottom | S1 and S4 |
| 103 | Middle | S1 and S4 |

The PPVs computed by models S1 to S4 are for some rows close and for some rows far from the PPVs measured in the field. In 0, the PPVs calculated by models S2 and S3 are close to the field measurements in cross-cut 100 top and middle rows, and models S1 and S4 provided closer results to field data in cross-cut 100 bottom row and cross-cut 103 middle row.

Since PPV alone was not enough to determine how well the models mimicked the real behaviour, other comparisons were performed. These analyses comprised comparison of:

i. The velocity-time graphs obtained from the field tests and calculated in UDEC.
ii. The displacement of the wall and the ejection from the wall obtained from the field monitoring data and numerical analyses.

### 4.2 Velocity-time comparison between field and UDEC models

The velocity-time graph recorded during field Test 6 in section *C* in cross-cuts 100 and 103 and those from the UDEC models are presented in 0a, b, c, and d. In 0, the accelerometers A2, A7, A13, and A19 are those installed in section *C*.

0 shows that for most of the models, the field and UDEC models are in the same order of magnitude and similar trend of graphs, resulting in a fair agreement between the graphs calculated by models and that recorded during the field test.

From 0 it can be observed that the velocity-time graphs recorded during field tests are characterized by a blunt peak followed by large duration after peak. By looking at 0a, b, and d, this type of behaviour can be observed in models S1 and S4 while models S2 and S3 are characterized with sharper peaks and a steeper post peak.

In 0c (bottom row of the test wall), certain differences can be observed between the overall trend of the graphs obtained in the field and those calculated in the UDEC. The graphs representing A12 and A13 are characterized by higher peak and longer duration compared to the graphs calculated in UDEC. The difference in the characteristics between the field experiment and the numerical analysis could be due to differences in length and location of the joints in the tested wall close to the bottom row. This can have resulted in more kinematic constraints at the bottom part of the cross-cut in the model than in the field test. In 0c, the PPV in models S1 and S4 are slightly closer to the field measurements.

In 0d, cross-cut 103 the middle row, velocity recorded by accelerometer A19 in Section *C* has a pronounced peak with a short duration followed by variations around 4.5 m/s. Thereafter the velocity decreases slowly with time. The velocity-time graphs calculated by UDEC models S1 and S4 have generally similar shapes as those measured in the field though there is a difference in the peaks of the graphs between field measurements and UDEC models. The velocity calculated in models S1 and S4 increases after about 4.0 ms and stays at a constant level for the rest of the simulation time.

Comparison of the field and UDEC velocity-time graphs shows that models S1 and S4 behave more similar to that in the field tests, than the other models.

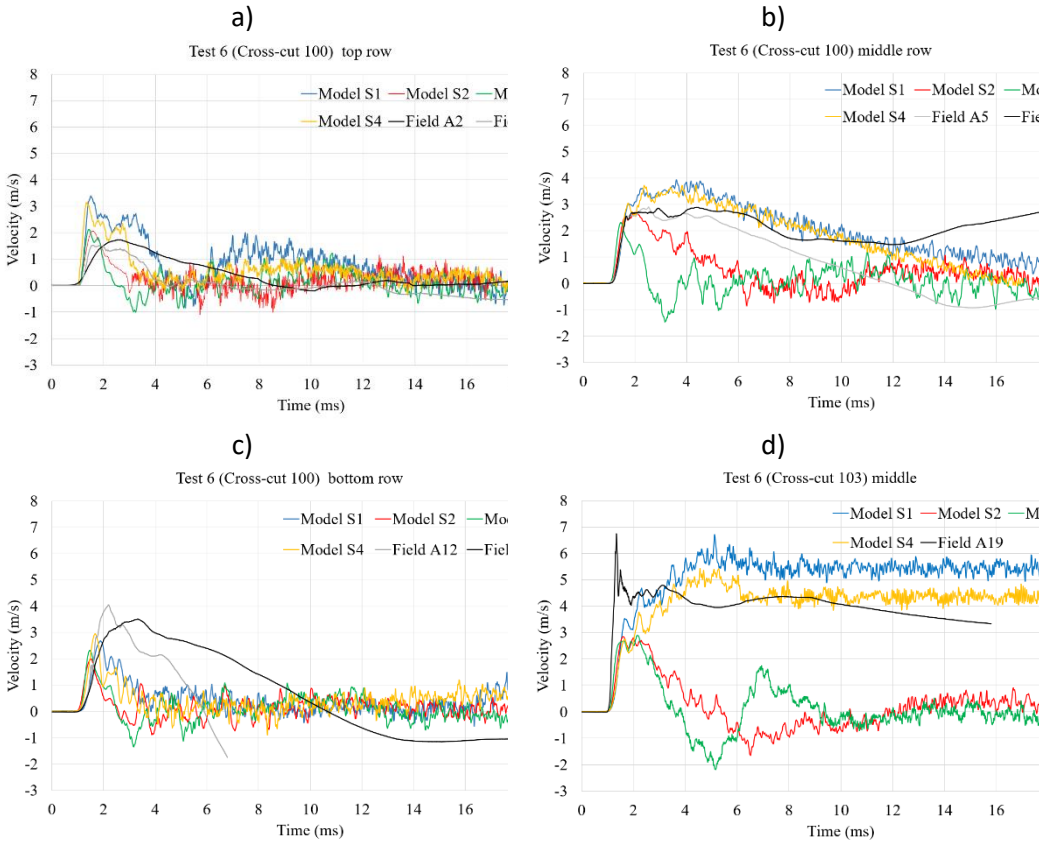


**Figure 10: Comparison of velocity-time graphs obtained in field Test 6 and UDEC models at a) top row cross-cut 100, b) middle row cross-cut 100, c) bottom row cross-cut 100, and d) middle row cross-cut 103.**

## 4.3 Displacement and ejection thickness

The calculated displacement and ejection thickness of the rock mass surrounding the burden and the test wall in cross-cuts 100 and 103 in models S1 – S4 were studied. This was to improve the understanding of the displacement variation over the height of the wall and thickness of the ejected material from the wall in cross-cut 103 in UDEC models. This, together with the velocity – times studied in previous section, were used to identify the model that behave most similar to the behaviour in the field measurements.

In the results presented in this section, the displacement is the inward movement of the test wall toward the tunnel. The displacements in the field were measured by scanning the surface of the test wall before and after blast. The ejection thickness is the ejected thickness or slab of the wall fall into the tunnel and the values were identified manually by measuring the ejected thickness on the test wall.

The results from the UDEC models in cross-cut 100 are summarized in 0a – d. The displacement of the wall in cross-cut 100 in models S1, S2 and S4 varied between 11 and 45 mm. A 90 mm failure thickness was developed at the surface of the test

wall in S1, S2 and S4. 0, shows that the failed thickness represents the movement of a very small block, which in a real cross-cut would have fallen out during drifting (blasting and scaling). Therefore, the displacement of the small wedge is not considered when the displacement of the wall is estimated for the model results. The displacement chosen to represent the overall movement of the wall is that of the wall above the small block.

According to Shirzadegan et al (2016b), the displacement range obtained in Test 6 cross-cut 100 was 1 – 26 mm. In cross-cut 100 in field Test 6, no severe damage to the support system was observed. The maximum visible damage in this cross-cut, reported by Shirzadegan et al. (2016b), occurred as debonding of shotcrete over an area of 1 m × 1 m of the test wall (close to the floor where the support ends).

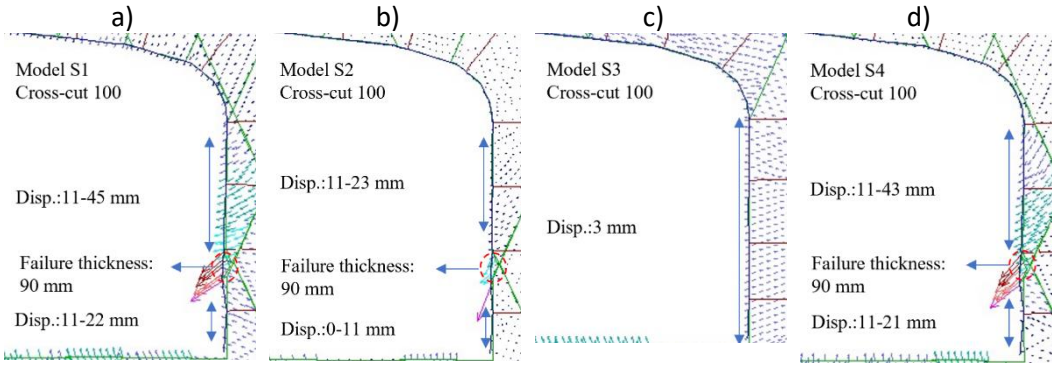


**Figure 11: Displacement and failure thickness in cross-cut 100 in models S1 – S4.**

In the UDEC models S1 and S4, the thickness of the ejected volume of rock in cross-cut 103 was 540 mm, see 0a – d. Models S2 and S3 did not show any ejection from the surface of the test wall.

According to Shirzadegan et al. (2016b), the ejection thickness in Test 6 cross-cut 103 was 100 – 800 mm. The test wall in cross-cut 103 failed to be functional and blocks of rock were ejected from the wall. The large pieces of rock and shotcrete lying in the centre of the cross-cut were ejected from a location 1.5–2 m above the floor and travelled a horizontal distance of about 2m.

From the UDEC analysis, it can be concluded that models S1 and S4 have mimicked the behaviour of cross-cuts 100 and 103 in Test 6 and they are better than the other models.

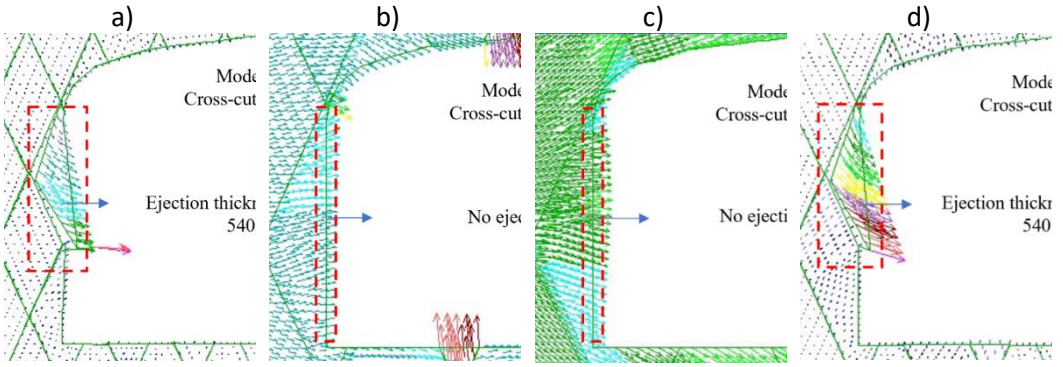


**Figure 12: Ejection thickness in cross-cut 103 in models S1 – S4.**

# 5. Rock mass and rock support response to dynamic loading

Models S1, with 0.6 m joint spacing between each joint set, was chosen to evaluate the design in field Test 6. For this purpose, the failure mechanism developed in the burden and over the height of the test wall is studied. Furthermore, the performance of rock support in the supported cross-cut, and the response of the test wall in the unsupported cross-cut are studied and presented in this section.

## 5.1 Behaviour of rock mass

### 5.1.1 Zones yielded in tension

The plastic state plots around cross-cuts 100 and 103 are used to study the failure mechanism in the burden. The results showed that, similar pattern of yielded zones in tension are distributed at the left- and right-hand side of the CZB toward the test walls in cross-cuts 100 and 103. In the presented plot in 0, the distribution of the zones yielded in tension have such features: (i) mainly concentrated around CZB, (ii) almost no yielded zone in the middle of the burden, and (iii) over the height of the wall of the cross-cuts 100 and 103.

The results from model S1 show that radial cracks are not developed in the middle part of the burden. The length of the extended yielded zones behind the wall surfaces are:

- 0.8 – 1.4 m in cross-cut 100, and
- 0.5 – 1.7 m in cross-cut 103.

Shirzadegan et al. (2016b) used observation boreholes with a diameter of 46 mm to identify the location of failure in the burden. These boreholes were filmed with a borehole camera, before and after the blast. The maximum depth of damage detected in field Test 6 was 0.6 m in cross-cut 100. In cross-cut 103, due to the ejection from the wall, the investigation of the observation borehole was not repeated after the blast. The ejection thickness in cross-cut 103, as mentioned in previous section, was up to 0.8 m.

The reason for difference in measured depth of damage between field test and the numerical model, is the difference between the size of the formed wedges behind the wall of the cross-cuts. From the results, it can be expected that smaller wedges existed in the test wall in cross-cuts 100 and 103. The reason is that since the UDEC model was 2D, only the dominant sets with strikes sub-parallel to the direction of the cross-cut are modelled. The formed wedges in the test wall in the field tests, are a combination of the all dominant and less frequent local joint sets.

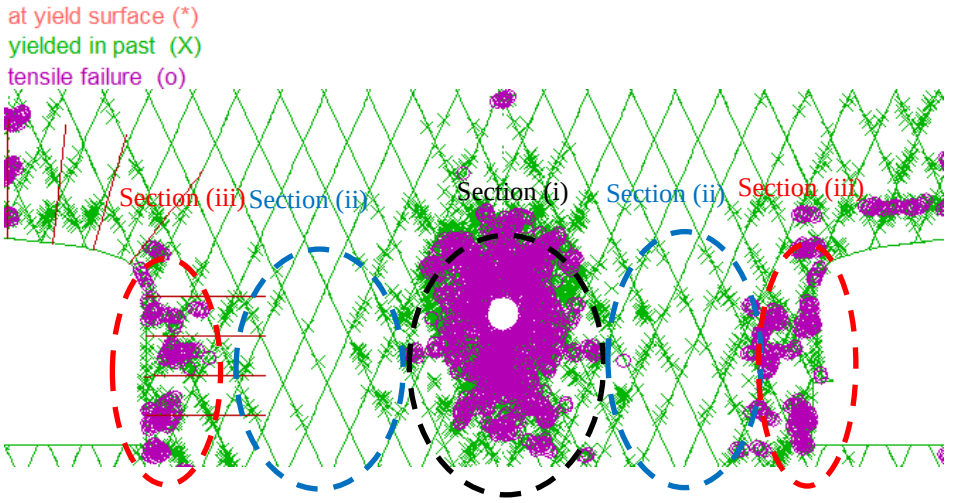


**Figure 13: Plastic state of the burden and the walls in cross-cuts 100 and 103 in numerical analysis of Test 6 in models S1.**

### 5.1.2 Wave propagation pattern

0a to d shows the evolution of the propagated wave in model S1 (burden = 7.7 – 8.9 m) to that in numerical model 1 of Test 4 (Shirzadegan 2020), with a burden of 2.8 m. Tests 4 and 6 are compared because similar charge diameter was used in both tests. The aim was to check the difference between the wave front radius in Tests 4 and 6 at the time when the wave reaches the test wall. The results show that, in Test 4, after 1 ms of wave propagation (0a), the wave has almost reached the wall, and at time 2 ms (0b), the wave front has passed the test wall. Due to the larger burden in Test 6, the wave has reached to the middle of the burden after 1 ms (0c), and time 2 ms, the wave arrives to the test wall (0d). As it can be observed in 0, the wave front in Test 6, has a larger radius, compared to that in Test 4, when it arrives at the test wall (after 2 ms of wave propagation).

Furthermore, Model S1 was also analysed with an additional blasthole in the model (according to the initial plan for Test 6). The new model is called Model S5. The wave front evolution in the model with two blastholes are presented in 0e and f. Comparison of the formed wave front at similar time intervals, indicates that the wave front has become slightly more planar compared to the model with 1 blasthole.

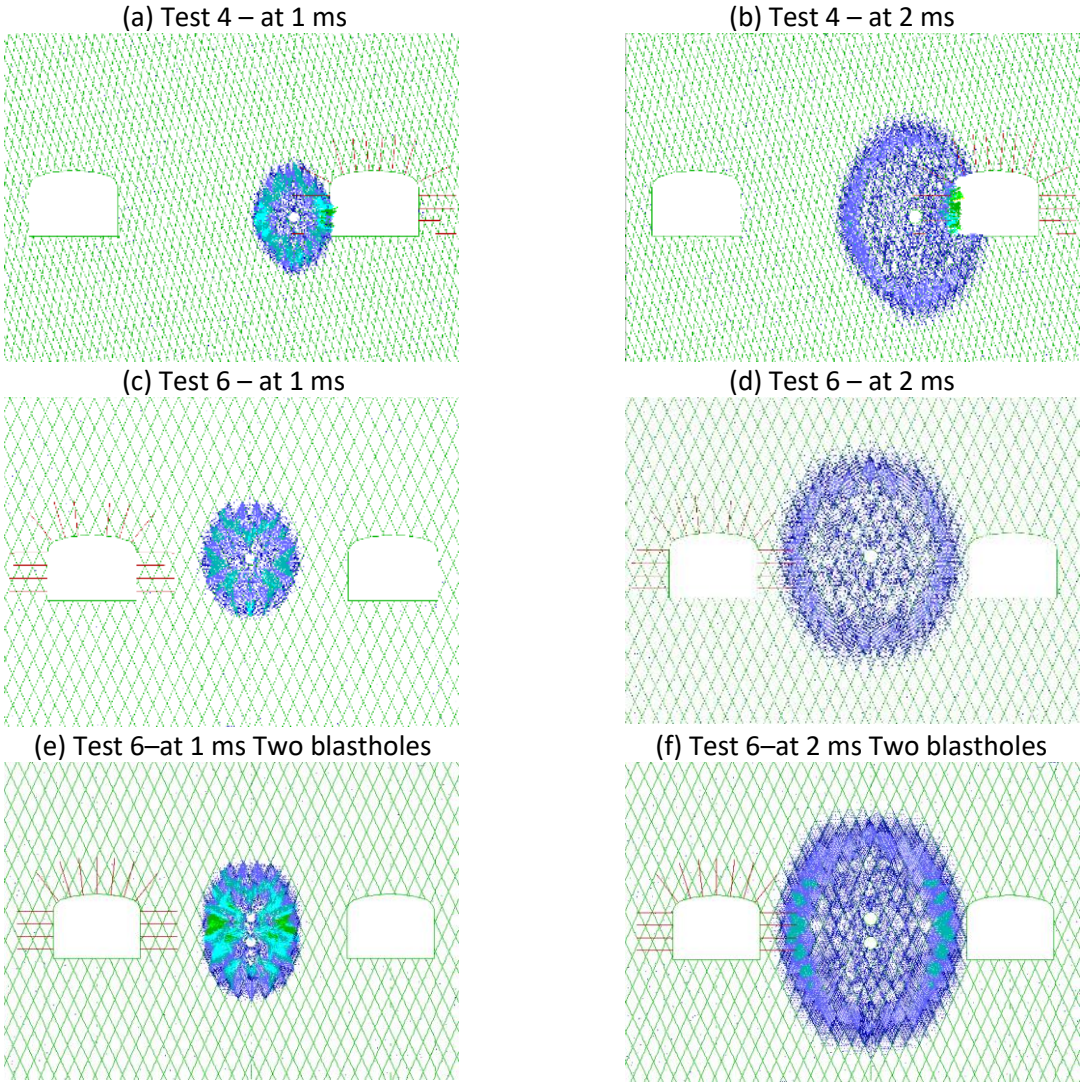


**Figure 14: Wave propagation pattern in Test 4 versus Test 6. a) – b): Test 4, c) – d): Test 6 with one blasthole (Model S1), e) – f): Test 6 with two blastholes (Model S5).**

## 5.2 Rock support performance

The performance of the installed rock support in cross-cut 100, was numerically analysed using the results obtained from model S1. The loading state of the rockbolts were investigated, and the possible failure modes were identified. The role of the installed rock support system on minimising the particle velocity, displacement and the extension of the yielded zones, is evaluated in this section.

### 5.2.1 Loading state of the rock support

Rockbolt breakage was observed for one of the elements of the marked rockbolts in 0a, closest to the surface of the test wall. The rest of the rockbolts in this cross-cut did not show any signs of breakage along their lengths. Rockbolt/rock interface failure was observed along the horizontal rockbolts installed at the right-hand side of cross-cut 100 and closest to the blasthole (see 0b). From the plot presented in 0b, it can be observed that except the marked rockbolt in 0b, rockbolt interface failure was induced only along minor intervals of the rockbolts in Model S1. The evidences from rockbolt breakage state and the interface failure along the rockbolts, confirm that the major part of the length of the rockbolts were still in active connection with the surrounding rock mass, the functionality of the rockbolts was maintained, and the ejection of the rock from the space between the rockbolts was avoided.

Shotcrete interface failure and axial (tensile) yielding developed all around the boundary of cross-cut 100 in model S1. The post-blast mapping of the test wall after conducting field Test 6 showed that, except at a few points on the tested wall, no severe damage to the shotcrete (spalling or creation of large cracks) was observed.

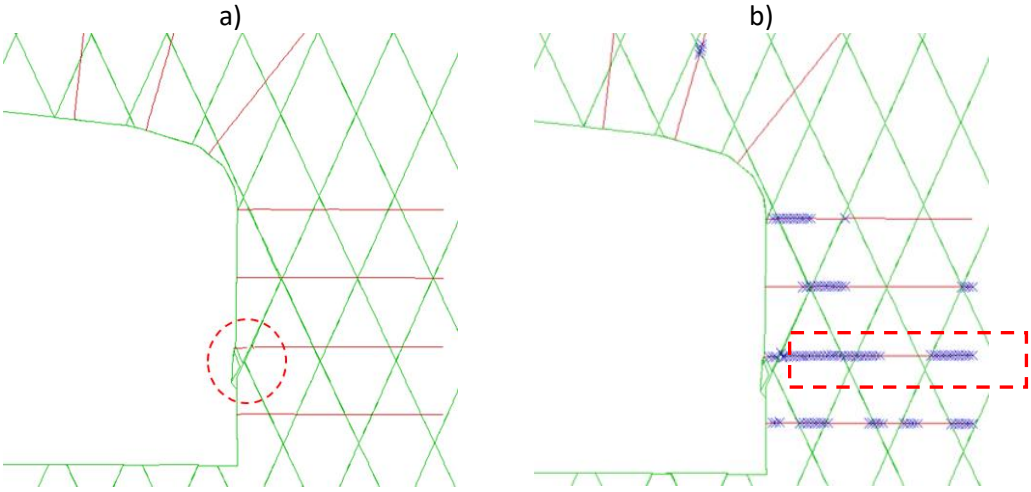


**Figure 15: a) Rockbolt breakage, b) interface failure.**

### 5.2.2 Effect of rock support on the excavation response

To numerically investigate the effect of the installed rock support in limiting the velocity and displacement, the support system from cross-cut 100 was removed, and cross-cut 103 was supported with the same rock support (Swellex and fibre reinforced shotcrete), used for cross-cut 100 in the earlier analyses. The new model is called S6. The velocity-time and displacement-time graphs of the Model S6 are compared with the initial support condition of the model S1.

The lack of the support in cross-cut 100 and the support of cross-cut 103 in Model S6, changed the PPV in the velocity-time graphs, see 0a and 0b. In 0, the result from Model S1 is shown in blue, and Model S6 in red colours. Lower PPV was calculated for the cases with the installed support system in the cross-cut 100 and 103.

Furthermore, the velocity – time graphs showed that the effect of rock support was evident in the overall trend of the graphs. The velocity showed only a small deceleration of the test walls in cross-cuts 100 and 103 without support. For the supported cases the deceleration started about 5 ms after the wave arrival.
The effect of the installed support system was also evident in the displacement – time graphs presented in 0a and 0b. The displacement was monitored at the mid-height of the wall for the cases of supported and unsupported cross-cut walls. The results show that in the supported case, the displacement increases asymptotically with cycling time and reaches a peak value after about 15 ms after the wave arrival, then it decreases and reaches a residual value, while the unsupported walls showed a constant acceleration with time.

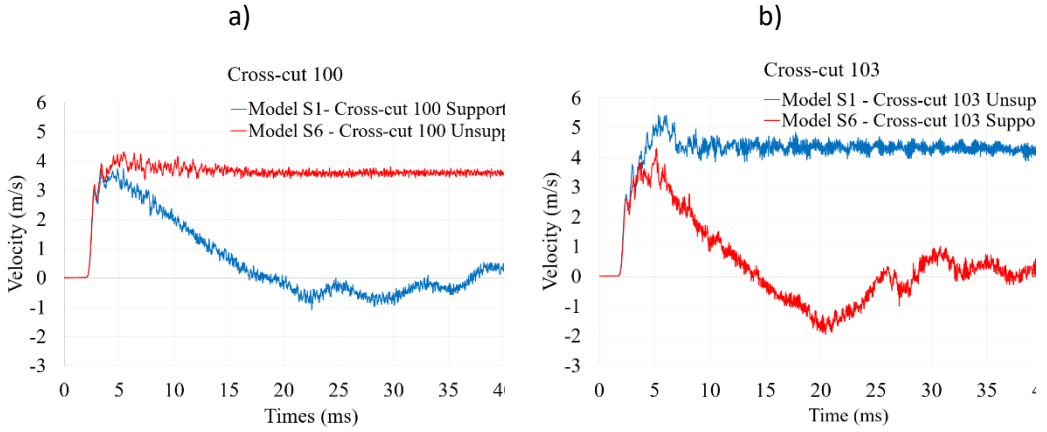


**Figure 16: Velocity-time curves for different support conditions in Models S1 and S6, a) cross-cut 100, b) cross-cut 103.**

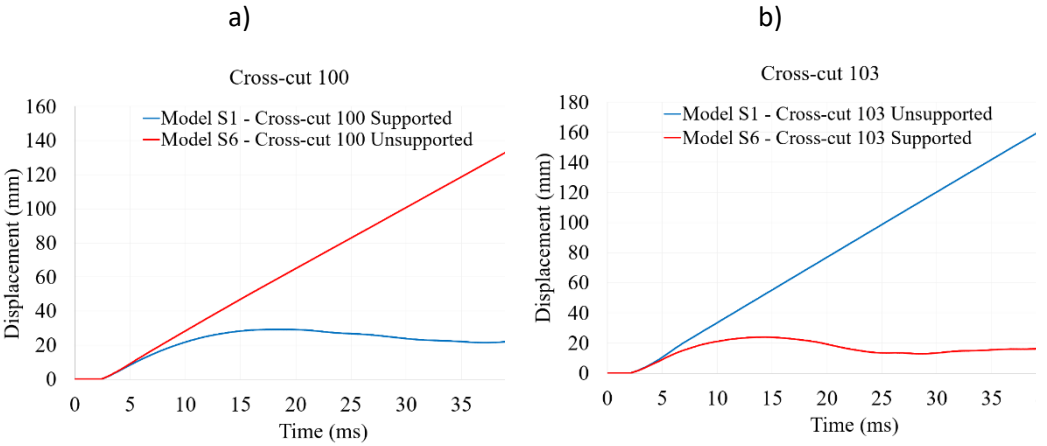


**Figure 17: Displacement-time curves for different support conditions in Models S1 and S6, a) cross-cut 100, b) cross-cut 103.**

## 6. Discussion

Test 6 and the numerical analysis was done to develop a field and a numerical method for testing of rock support. In this study, four discontinuous numerical models were developed by using the joint sets identified during field mapping. The joint spacing was varied between the different models. The results of the four numerical models were further investigated by comparing, the velocity – time graphs, and displacement range, to those obtained in field Test 6. Model S1 with the joint spacing showing the best agreement (in velocity and displacement) with the field Test 6 results, was then used to study the performance of the new burden design in Test 6 and the performance of the installed rock support.

The new design, used for Test 6, aimed at avoiding the development of radial cracks that propagate from the blasthole the whole way to the test wall surface. By doing so, the development of a wedge-shaped volume that can be ejected (complete damage of the burden), was prevented. This aim was achieved since no such radial fractures can be observed in the UDEC models. In this numerical study, the plot of the plasticity state was used to identify the locations of yielded zones in the model. The yielded zones were interpreted as the location of potential cracks. The development of the zones yielding in tension was limited to the areas around the blasthole, and in the rock close to the surface of the tested wall. The results show that the increased burden has effectively minimized the area of yielding in tension (propagated radial cracks) in the middle section of the burden. The explanation to this is firstly, that the increased burden has resulted in more geometrical attenuation (compared to that in Tests 1 to 5) during its propagation from the blasthole to the tested walls. Consequently, in the middle section of the burden, the induced tangential stresses did not exceed the tensile strength of the rock mass. Therefore, the areas of tensile yielding caused by the incident wave did not develop. Secondly, the energy carried by the reflected wave was absorbed by fracturing of the rock (tensile yielding zones), displacement along discontinuities, stretching of the rockbolts, and fracturing of the shotcrete in cross-cut 100. The reflected wave from the surface of the opening was therefore attenuated before reaching to the mid-section of the burden in Test 6. As a result, the tensile yielding zones caused by the reflected wave in the mid-section of the burden were not created, i.e., no formation of radial cracks in the burden avoiding the creation of the wedge-shaped volume and complete damage of the burden.

The depth of damage in field Test 6, was estimated by using a borehole camera. The measured depth of damage in the field was less than that measured in the numerical model. The first explanation to this difference can be the actual geological condition behind in the test wall, which is different from a numerical model that has limitations and uses assumptions. The second source of difference, can be due to the limitations of the used instrument for detecting the depth of failure in the wall in the field. Measurement by the borehole camera was performed in 46 mm diameter observation boreholes before and after the blast. Before the blast, it was possible to send the camera all the way inside the 3 m meter long drilled boreholes. After the

blast, the camera was stopped in the boreholes where a breakage or a movement along the joints in the wall had occurred. This is while the real damage in the wall in the field may be farther from the wall surface, since the camera was stuck at some of the shallowest damages. Furthermore, the number of drilled boreholes were limited to eleven. From the plastic state plot in UDEC, it is possible to measure the whole length of the extended tensile failure. It should also be noted that, eleven observation boreholes were drilled over an area of 20 m (length) * 4 m (height) of the test wall. Although the number of the drilled boreholes were sufficient in the field test, it is always possible that the coordinates of the developed failure in the wall in the field and the UDEC model do not coincide.

The level of the rock support damage in the numerical analysis of cross-cut 100 and the ejection from the unsupported wall in cross-cut 103, were in agreement with the level of damage observed after field Test 6; i.e. minimum damage to the support system in cross-cut 100, and ejection from the wall of cross-cut 103. The numerical analysis results suggest that the installed support system has played an important role in distributing the dynamic load, limiting the displacement, and as a result, prevented ejection and fallouts in cross-cut 100. Since the blasthole in Test 6 was drilled in the middle of the pillar between the two cross-cuts, it was concluded that the difference in behaviour of cross-cut 100 and 103 was due to the effect of the rock support installed in cross-cut 100. Therefore, Model S6 was developed in which the rock support was installed in cross-cut 103 and cross-cut 100 was left unsupported. The numerical analysis of the Model S6 and the comparison of the results with original S1 confirmed this conclusion.

Shirzadegan et al. (2016b) calculated the kinetic energy contained in the ejected blocks of rock in cross-cut 103, and classified the level of damage in this cross-cut as the “high damage intensity”, according to the rockburst damage classification proposed by Kaiser et al. (1996). By modelling the rock support in cross-cut 103, it was observed that the ejection from the wall is prevented in this cross-cut. This again confirms the conclusion that the used support system has the capacity to be used in burst prone areas of the mine, where high damage intensity to the opening is expected.

Large scale tests of rock support are costly, and the setup and design process of the tests requires large amount of time and collaboration between different sectors of mines and the research team. However, according to the experience gained from field tests (Shirzadegan et al., 2016a; Shirzadegan et al., 2016b), the major challenge was the optimum design of the burden with respect to the amount of used explosives. Performing forward numerical analysis will lead to an optimum design and assist in finding the useful pattern for distribution of monitoring instruments over the surface of the test wall. When the results from field tests are available, the backward numerical analysis will assist in better understanding the rock mass behaviour and support response to the designed dynamic loading. As the geological conditions of the test site have an important role in controlling the level of damage to the burden and the tested wall, it is important to have a good knowledge of the geological condition of the site before conducting the test.

## 7. Conclusions

This paper presents the results from the numerical analysis of the large-scale dynamic test of rock support, Test 6, conducted at the LKAB Kiirunavaara mine. The analysis provided insight into the response of the rock, and performance of support system to the dynamic loading. The major conclusions of the numerical analysis of field Test 6 are:

- The pattern of the developed tensile failure between the blasthole and the surface of the test wall, confirmed that the larger burden, has assisted in avoiding the tensile yielding in the middle parts of the burden, and as a result prevented complete damage of the burden. The zones yielded in tension were only concentrated around the blasthole and close to the surface of the cross-cut. The results showed that the larger the distance between the blasthole and the test wall, the chances of producing a more planar wave front, will be increased.
- The differences that were observed between the field collected data and the numerical analysis results can be attributed to the nature of the monitoring instruments and differences between the actual site geological conditions and those used in the UDEC models. Despite the differences, the field tests results and the numerical analysis results were in acceptable agreement.
- The installed rock support, Swellex Mn 24 and reinforced shotcrete, was effective in limiting the damage in the wall of the opening and prevent ejection. The support system showed that it has the capacity to be used in burst prone areas of the mine. The results showed that the lack of the presence of the used support could result in ejection from the wall.
- To evaluate rock support performance under dynamic loading conditions, it is possible to conduct large-scale tests of rock support. The major challenge in the tests is to design the burden. Performing numerical analysis can significantly save time and energy while searching for an optimum design of the burden. By using a calibrated numerical model, it is possible to test the performance of different support systems using the same boundary conditions in future studies.

## Acknowledgements

This work was financially supported by LKAB, Boliden and Centre of Advanced Mining & Metallurgy at LTU (CAMM) and the I2Mine project which are gratefully acknowledged. The LKAB Mining Company in Kiruna is gratefully acknowledged for providing the opportunity to conduct the tests at this mine.

## References

[1] Andersson, U.B. (2011). Tättkartering runt skjutskador ort 93 oh 95 Z741. Internal Report LKAB Kiruna, Sweden.
[2] Andersson, U.B. (2010). Geology and Structures for Level Z741 Blocks 9 and 12. Internal Report LKAB Kiruna, Sweden.
[3] Andrieux, P.P., Turichshev, A., O´Connor, C.P. and Brummer, R.K. (2005). Dynamic Testing With Explosive Charges of Rockburst-Resistant Ground Support Systems at the Fraser Nickel.
[4] Mine. Report to Falconbridge Limited Mine Technical Services, Final Version, September 2005 Itasca Consulting Company Inc. Sudbury, Canada.
[5] Ansell, A. (2004). In situ testing of young shotcrete subjected to vibrations from blasting. Tunnelling and Underground Space Technology, 19(6):587-596
[6] Ansell, A. (1999). Dynamically loaded rock reinforcement. (Publication No. diva-2876 ) [Doctoral Dissertation, Institutionen för byggkonstruktion - KTH ]
[7] Archibald, J.F., Baidoe, J.P., and Katsabanis, P.T. (2003). Rockburst damage mitigation benefits deriving from use of spray-on rock lining. In: Potvin Y, Stacey, T.R., Hadjigeorgiou, J. (eds). Proceeding of third international seminar on surface support liners: Thin spray-on liners, shotcrete and mesh, Universite´ Laval, Quebec City, Canada, August 2003 Section 19 pp. 169-178.
[8] Barla, G., Monacis, G., Perino, A., and Hatzor, Y. (2010) Distinct element modelling in static and dynamic conditions with application to an underground archaeological site. Journal of Rock Mechanics and Rock Engineering 43(6):877-890.
[9] Borrvall, T., and Riedel, W. (2011). The RHT concrete model in LS-DYNA. In: Proceedings of the 8th european LS-DYNA users conference, Strasbourg,France.
[10] Brandshaug, T. (2009). An Initial Evaluation of the Effects of Seismic Motion on a Footwall Drift at LKAB's Kiirunavaara Mine. GT09-4001-1 LKAB Kiirunavaara mine.
[11] Chen, S.G., and Zhao, J. (1998). A study of UDEC modelling for blast wave propagation in jointed rock masses. International Journal of Rock Mechanics and Mining Sciences 35(1):93-99.
[12] Chen, S.G., Zhao, J., and Zhou, Y.X. (2000). UDEC modeling of a field explosion test. International Journal for Blasting and Fragmentation 4(2):149-163.
[13] Chong, K., Zhou, Y., Seah, C., and Lim, H.S. (2002). Large-scale tests — airblast, ground shock, and debris. In: Proceedings of the international symposium on defence construction, Singapore, pp. 17-18.
[14] Deng, X.F., Chen, S.G., Zhu, J.B., Zhou, Y.X., Zhao, Z.Y., and Zhao, J. (2015). UDEC–AUTODYN hybrid modeling of a large-scale underground explosion test. Rock Mechanics and Rock Engineering 48(2):737-747.

[15] Espley, S.J., Heilig, J., and Moreau, L.H. (2002). Assessment of the dynamic capacity of liners for application in highly-stressed mining environments at INCO Limited. In: Potvin Y, Stacey TR, Hadjigeorgiou J (eds) Proceedings of the international seminar on surface support liners, Johannesburg, South Africa, July 2002 pp. 187-192.
[16] Hadjigeorgiou, J., and Potvin, Y. (2007). Overview of Dynamic testing of Ground Support. In: Potvin Y (eds) Proceeding of the 4th international seminar on 'Deep and high stress mining, Australian Centre for Geomechanics, Perth, pp. 349-371.
[17] Hagan, T.O., Milev, A.M., Spottiswoode, S.M., Hildyard, M.W., Grodner, M., Rorke. A.J., Finnie, G.J., Reddy, N., Haile, A.T., and Le Bron, K.B. (2001) Simulated rockburst experiment-an overview. Journal of the Southern African Institute of Mining and Metallurgy 101(5):217-222.
[18] Hallquist, J.O. (2006). LS-DYNA theory manual. Livermore, California:
[19] Heal, D. (2010). Observations and analysis of incidences of rockburst damage in underground mines. [Unpublished Doctoral Dissertation ] University of Western Australia.
[20] Heal, D., and Potvin, Y. (2007). In-situ Dynamic Testing of Ground Support Using Simulated Rockburst. In: Potvin Y (eds) Proceeding of fourth international seminar on 'deep and high stress mining', Australian Centre for Geomechanics, Perth, Australia, pp. 373-394.
[21] Heal, D., Hudyma, M., Langille, C., Potvin, Y., Butcher, R., Ball, R., and Hartmann, B. (2005). In-situ testing of ground support performance under strong dynamic loading. In: Potvin Y, Hudyma M (eds) Proceedings of the 6th international symposium on rockbursts and seismicity in mines, Australian Centre for Geomechanics, Perth, Australia, pp. 85-94.
[22] Helte, A., Lundgren, J., Örnhed, H., and Norrefeldt, M. (2006). Prestandabestämning av svensk sprängdeg m/46.( Report nr FOI-R--2051)--SE Stockholm.
[23] Itasca Consulting Group (2015). UDEC-Universal Distinct Element Code, Version 6.0, User Manual, Minnesota, USA.
[24] Kaiser, P.K., MacCreath, D.R., and Tannant, D.D. (1996). Canadian rockburst support handbook. Sudbury, Ontario, Canada.: Geomechanics Research Centre.
[25] Kuhlemeyer, R.L., and Lysmer, J. (1973). Finite element method accuracy for wave propagation problems. Journal of Soil Mechanics & Foundations Div 99(Tech Rpt).
[26] Lemos, J. (1997). A distinct element model for dynamic analysis of jointed rock with application to dam foundations and fault motion.[Doctoral Dissertation, University of Minnesota].
[27] Malmgren, L. (2008). Design basis - Kiirunavaara mine. Internal report LKAB Kiirunavaara LKAB mine.
[28] Malmgren, L. (2007). Strength, ductility and stiffness of fibre-reinforced shotcrete. Magazine of Concrete Research 59(4):287-296.

[29] Malmgren, L., and Nordlund, E. (2008). Interaction of shotcrete with rock and rock bolts - A numerical study. International Journal of Rock Mechanics and Mining Sciences 45(4):538-553.
[30] Malmgren, L., and Nordlund, E. (2006). Behaviour of shotcrete supported rock wedges subjected to blast-induced vibrations. International Journal of Rock Mechanics and Mining Sciences 43(4):593-615.
[31] Malmgren, L., and Sjöberg, J. (2006). Bergmekaniska analyser för ny huvudnivå i KUJ (1365). Utredning nr 06-797 LKAB Sweden
[32] Olovsson, L., Souli, M., and Do, I. (2003). Fluid-structure interaction capabilities in LS-DYNA.
Http://Ftp.Lstc.Com/Anonymous/ Outgoing/Jday/Aletutorial-278p.Pdf
[33] Ortlepp, W. (1992). The design of support for the containment of rockburst damage in tunnels–an engineering approach. In: Proc. int. symp. on rock support in mining and underground construction, pp. 593-609.
[34] Ortlepp, W. (1969). An empirical determination of the effectiveness of rockbolt support under impulse loading. In: Brekke TL, Jorstad FA (eds) Proceedings of the international symposium on large permanent underground openings, Universitats - forlaget, Oslo, Norway, pp. 197-205.
[35] Potvin, Y., Wesseloo, J., and Heal, D. (2010). An interpretation of ground support capacity submitted to dynamic loading. In: Van Sint Jan M, Potvin Y (eds) Proceedings of the 5th international seminar on deep and high stress mining, Australian Center for Geomechanics, Santiago, pp. 251-272.
[36] Riedel, W., Thoma, K., Hiermaier, S., and Schmolinske, E. (1999). Penetration of reinforced concrete by BETA-B-500 numerical analysis using a new macroscopic concrete model for hydrocodes. In: Proceedings of the 9th international symposium on the effects of munitions with structures, Berlin-Strasburg.
[37] Rosengren, L. (1993). Preliminary analysis of the dynamic interaction between Norra Länken and a subway tunnel for Stockholm, Sweden. Tunnelling and Underground Space Technology 8(4):429-439.
[38] Saiang, D., Malmgren, L., and Nordlund, E. (2005). Laboratory tests on shotcrete-rock joints in direct shear, tension and compression. Journal of Rock Mechanics and Rock Engineering 38(4):275-297.
[39] Senseny, P.E., and Simons, D.A. (1994). Comparison of calculational approaches for structural deformation in jointed rock. International Journal for Numerical and Analytical Methods in Geomechanics 18(5):327-344.
[40] Shirzadegan, S. (2020). Development of a Methodology for Dynamic Testing of Rock Support – Field tests and numerical analysis.(Publication No. diva-81197) [Doctoral Dissertation, Luleå University of Technoogy].
[41] Shirzadegan, S., Nordlund, E., and Zhang, P. (2016a). Large scale dynamic testing of rock support system at Kiirunavaara underground mine. Journal of Rock Mechanics and Rock Engineering 49(7):2773-2794.

[42] Shirzadegan, S., Nordlund, E., and Zhang, P. (2016b). Large scale dynamic testing of rock support at Kiirunavaara – Improved test design. Tunneling and Underground Space Technology 59:183-198.
[43] Stacey, T. (2012). A philosophical view on the testing of rock support for rockburst conditions. Journal of the Southern African Institute of Mining and Metallurgy ISSN 2411-9717, 112(8):703-710.
[44] Stacey, T. (2011). Support of excavations subjected to dynamic (rockburst) loading. In: Qian Q, Zhou Y (eds) Proceedings of the 12th international congress of the international society of rock mechanics, pp. 137-145..
[45] Tannant. D.D., Brummer, R.K., and Yi, X. (1995). Rockbolt behaviour under dynamic loading: field tests and modelling. International Journal of Rock Mechanics and Mining Sciences & Geomechanics Abstracts 32(6):537-550.
[46] Tannant, D.D., McDowell, G.M., and McCreath, D.R. (1994). Shotcrete performance during simulated rockbursts. In: Workshop on applied rockburst research (eds) IVth south american congress on rock mechanics, (SOCHIGE), Santiago, pp. 241-248.
[47] Wang, Z.L., Konietzky, H., and Shen, R.F. (2009). Coupled finite element and discrete element method for underground blast in faulted rock masses. Soil Dynamics and Earthquake Engineering 29(6):939-945.
[48] Wu ,T.H. (1971). Soil dynamics. Boston, MA United States: Allyn and Bacon, Incorporated.
[49] Zhang, P., Yi, C.P., Nordlund, E., Shirzadegan, S., Nyberg, U., Malmgren, L., and Nordqvist, A. (2013). Numerical back analysis of simulated rockburst field tests by using coupled numerical technique. In: Potvin Y (eds) Proceeding of seventh international symposium on ground support in mining and underground construction, Australian centre for Geomechanics, Perth, pp. 565-585.
[50] Zhao, X., Zhao, J., Cai, J., and Hefny, A. (2008). UDEC modelling on wave propagation across fractured rock masses. Computers and Geotechnics 35(1):97-104.